# Attoclock with counter-rotating bicircular laser fields

Nicolas Eicke[*] and Manfred Lein

*Institut für Theoretische Physik, Leibniz Universität Hannover, Appelstraße 2, 30167 Hannover, Germany*

The attoclock technique which maps the emission time of a photoelectron to its detection angle is an important tool in strong-field physics. Previously, it was implemented only with circularly or elliptically polarized laser fields. Here, we show how counter-rotating bicircular laser fields can be used as an attoclock to investigate the ionization dynamics in quasilinear polarization. This is achieved by choosing the ratio of the two field strengths in a way such that the vector potential has aspects of the attoclock and time is mapped directly to the photoelectron momentum, but the shape of the electric field corresponds to approximately linear polarization during three intervals per optical cycle. We report momentum distributions calculated by solving the time-dependent Schrödinger equation for a model helium atom and obtain the mapping from photoelectron momentum to ionization time using a trajectory-free method. Unlike circular polarization where the time of maximal ionization rate typically deviates less than 5 attoseconds from the maximum of the electric field, we find positive ionization times of more than 10 attoseconds in the quasilinear case.

Attosecond angular streaking, or the "attoclock," allows us to probe the ionization process in strong laser fields with attosecond precision. It exploits the fact that in strong-field above-threshold ionization (ATI) of atoms with circularly polarized laser fields, the ionization time of the photoelectron is mapped to its detection angle. First implemented by Eckle *et al.* [1], it was subsequently used to probe ionization time delays, Coulomb effects, spatial properties of the tunnel barrier, and multielectron effects [2–10]. Detailed knowledge about the ionization step is important as it is the first part of the three-step process that leads to high-harmonic generation (HHG) and laser-induced electron diffraction or rescattering [11–17], and to set the initial conditions for trajectory-based models of strong-field ionization [18–20].

In the adiabatic tunneling regime, characterized by a small Keldysh parameter $\gamma = \sqrt{2I_p}\,\omega/E \ll 1$, where $I_p$ is the ionization potential of the atom, $\omega$ is the frequency of the laser field and $E$ its amplitude, the ionization step does not depend on the shape of the field [21,22]. In this case, the use of circularly polarized laser fields in the attoclock is not a limitation. This is different in the frequently visited regime of nonadiabatic tunnel ionization ($\gamma \lesssim 1$). For example, the strong-field approximation (SFA) in saddle-point approximation [23,24] predicts for linear polarization a symmetric distribution of initial velocities of the photoelectron perpendicular to the direction of the instantaneous electric field and nonvanishing parallel velocities [18], but for circular polarization an asymmetric distribution of initial perpendicular velocities and vanishing parallel velocities [25]. These nonadiabatic effects are observable in the photoelectron momentum distribution (PMD) as an enhancement toward the classical cutoff in linear polarization [26] or a disagreement of the measured photoelectron energy with the ponderomotive energy in circular polarization, as well as an asymmetry of ionization rates

between co- and counter-rotating atomic *p* orbitals [25,27]. These considerations lead to the question how the attosecond temporal structure in linear polarization can be retrieved by an experimentally feasible scheme. Although the SFA provides a simple time-to-momentum mapping also for linear polarization, the concept of the attoclock cannot be transferred directly (e.g., to answer the question whether the time of peak field stength corresponds to the maximum of the instantaneous ionization rate). The part of the PMD that corresponds to ionization at the peak of the pulse is centered around zero momentum and thus dominated by Coulomb effects [28–31]. Also, the occurrence of intracycle interference spoils the signal from a single ionization time [32,33]. Although other methods have been developed that can relate features of the PMD (or harmonic spectrum) in linear polarization to the time of ionization, such as parallel [34–36] and orthogonal [37–40] two-color schemes, ionization times around the peak or ascending part of the field have stayed inaccessible so far. Furthermore, the direct-ionization spectrum around the classical cutoff is not easily accessible as it overlaps with the onset of the rescattering plateau [41].

There is thus a true need to devise an approach for cleaner investigation of the time structure of ionization in linear polarization. In this work we demonstrate that the ionization step in (almost) linear polarization can be probed using an attoclocklike setup involving bicircular fields [42], which have already been used successfully to investigate various aspects of strong-field ionization [43–49]. The term bicircular field refers to the superposition of two circularly polarized fields with different wavelength. Specifically, we use counter-rotating $\omega-2\omega$ fields. In this "bicircular attoclock," time is not mapped to angle, as is the case for the circular attoclock, but to a shift in the momentum distribution in the direction perpendicular to the momentum where the distribution peaks. In this way we also avoid ambiguities due to geometrical effects that impede a clear definition of the relevant offset angle in the conventional attoclock [50,51]. As it turns out,

_____
*nicolas.eicke@itp.uni-hannover.de

the bicircular attoclock comes with another great benefit as the overall shape of the PMD provides directly the relative phase of the $\omega - 2\omega$ field.

We solve the two-dimensional time-dependent Schrödinger equation (TDSE)

$$i\frac{\partial}{\partial t}|\psi(t)\rangle = \left(\frac{1}{2}[\mathbf{p} + \mathbf{A}(t)]^2 + V\right)|\psi(t)\rangle \qquad (1)$$

for the soft-core potential

$$V(\mathbf{r}) = \frac{-1}{\sqrt{\mathbf{r}^2 + \alpha}}, \qquad (2)$$

where $\alpha \approx 0.0684$ is chosen to reproduce the ionization potential $I_p = 0.904$ a.u. of the helium atom (atomic units are used unless stated otherwise). We solve the TDSE using the split-operator method with time step 0.004 a.u. on a Cartesian grid with 2048 points in each dimension and a box size of $300 \times 300$ a.u. To obtain the momentum distribution, outgoing parts of the wave function are projected onto Volkov states via an absorber that starts at a distance of 100 a.u. from the center [52]. The vector potential

$$\mathbf{A}(t) = -\frac{2}{\sqrt{5}}\frac{E_0}{\omega}\left[\begin{pmatrix} \cos(\omega t) \\ \sin(\omega t) \end{pmatrix} + \frac{1}{4}\begin{pmatrix} -\cos(2\omega t) \\ \sin(2\omega t) \end{pmatrix}\right] \qquad (3)$$

describes a counter-rotating bicircular field with field-strength ratio 2:1 of fundamental to second harmonic and time-averaged intensity $c\,\epsilon_0\,E_0^2$. The ratio is chosen in a way that the field approximates a linearly polarized field near its peak three times per optical cycle of the fundamental $\omega$ field. In particular, close to $t = 0$ we can expand

$$\mathbf{E}(t) = \frac{3E_0}{\sqrt{5}}\begin{pmatrix} 0 \\ 1 - \frac{1}{2}(\sqrt{2}\,\omega)^2 t^2 \end{pmatrix} + O(t^3), \qquad (4)$$

which corresponds to linear polarization along the $y$ axis with peak field strength $E_{\text{peak}} = 3E_0/\sqrt{5}$ and effective frequency $\omega_{\text{eff}} = \sqrt{2}\,\omega$. We choose $\omega_{\text{eff}} = 0.05695$ a.u. such that the bicircular field approximates linear polarization at 800 nm. Therefore, the actual wavelength of the fundamental field is approximately 1131 nm. While the counter-rotating bicircular field can be used to mimic linear polarization, a corotating bicircular field is not considered because it resembles elliptical polarization in the vicinity of the maximum, similar to the conventional attoclock. In the TDSE calculations we modify the vector potential (3) with an envelope $f(t) = \cos^4(\omega t/6)$ (three-cycle pulse) to avoid the appearance of ATI rings in the PMD.

The vector potential and the electric field $\mathbf{E}(t) = -\partial_t \mathbf{A}(t)$, together with an example momentum distribution calculated in SFA are depicted in Fig. 1(a). The momentum distribution exhibits three distinct maxima corresponding to the three regions of almost linear polarization. The SFA provides a natural time-to-momentum mapping $t_s \mapsto \mathbf{p}$ via the saddle-point equation

$$\frac{1}{2}[\mathbf{p} + \mathbf{A}(t_s)]^2 + I_p = 0. \qquad (5)$$

Usually, this is solved for the complex ionization time $t_s$, given the momentum $\mathbf{p}$ (see [43,44] for an extensive analysis of PMDs of atoms in bicircular fields in the framework of the SFA). For the present purpose it is convenient to use the inverse mapping

$$\mathbf{p} = -\text{Re}\mathbf{A} \pm \text{Im}\mathbf{A}_\perp \sqrt{1 - \frac{2I_p}{(\text{Im}\mathbf{A})^2}}, \qquad (6)$$

where $\mathbf{A}_\perp = (A_y, -A_x)$. This maps a line of fixed real part of the ionization time and variable imaginary part directly to the "hand of the clock." A few of these lines are shown in Fig. 1(a). In contrast to the conventional attoclock where
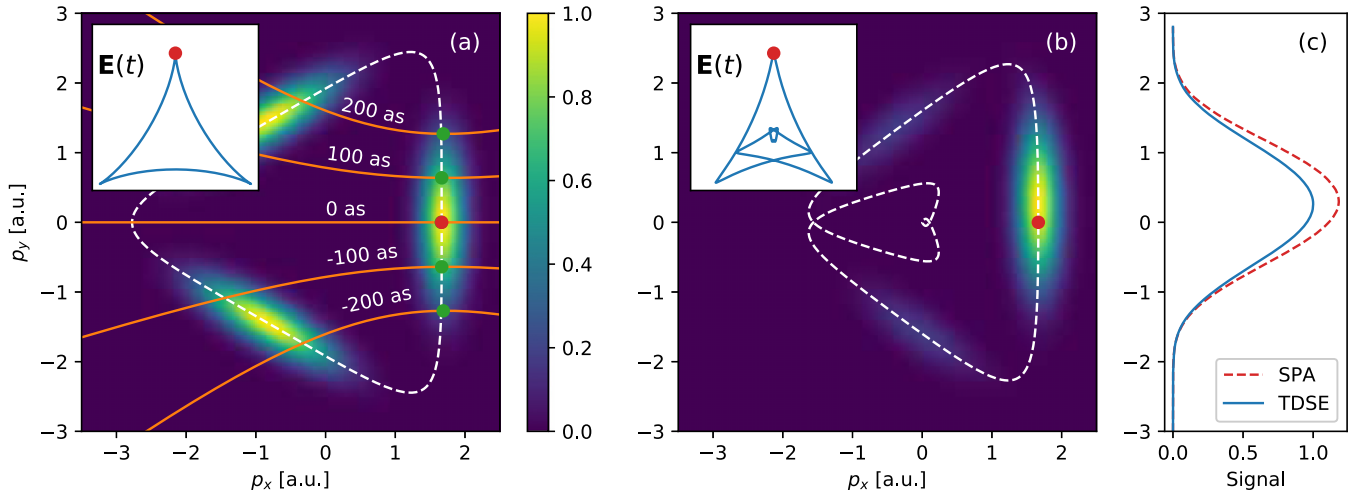


FIG. 1. (a) Shape of the electric field (inset), negative vector potential (dashed white line), and momentum distribution as obtained in the SFA for a continuous-wave field with $E_0 = 0.10$ a.u. The orange lines give the "hand of the clock," i.e., the momenta that are associated with a given real part of the ionization time. The green dots join the two branches of solutions of the quadratic saddle-point equation (5) and have minimal imaginary part. (b) Momentum distribution calculated by numerical solution of the TDSE for a short pulse, but otherwise the same parameters as in (a). (c) Slice through the maximum of the PMD. The blue solid curve gives the TDSE result from (b) and the red dashed curve is the signal obtained by applying the saddle-point approximation to the Dyson integral (11). Distributions in (a) and (b) are normalized to maximum signal 1. The saddle-point signal reaches a slightly higher maximum value of 1.18 times the maximum signal obtained directly from the TDSE.

time is mapped to angle, we see that in the vicinity of $t = 0$ [indicated by the red dot in Fig. 1(a)], time is mapped to the $p_y$ component of the photoelectron momentum. Because of the forward-backward symmetry of the vector potential, the speed of the clock must be an even function of time and thus it is constant to first order at the peak of the field. Using that the $p_x$ value of the maximum closely follows the classical value $-\mathbf{A}(t)$ at peak field strength [see the dashed line in Fig. 1(a)],

$$p_x^{\max} = \frac{E_{\text{peak}}}{2\omega}, \tag{7}$$

one obtains for the relative shift in the $p_y$ direction approximately (see Appendix A)

$$\frac{1}{p_x^{\max}} \frac{dp_y}{dt} = 2\omega\sqrt{1 + \gamma_{\text{eff}}^2}, \quad \gamma_{\text{eff}} = \frac{\sqrt{2I_p}\,\omega_{\text{eff}}}{E_{\text{peak}}}. \tag{8}$$

Here, $\gamma_{\text{eff}}$ is the effective Keldysh parameter at peak field strength. This is different from the circular attoclock where the speed of the clock is given simply by the angular frequency $\omega$. The factor of 2 can be understood as a combination of two effects: (i) the $2\omega$ component makes the clock go faster; (ii) the maximum of the PMD is found at smaller momenta because the two components of the vector potential point in opposite directions at peak field strength [see Eq. (7)]. The factor involving the Keldysh parameter is due to nonvanishing parallel exit velocities that arise in nonadiabatic tunnel ionization in SFA in linear, but not in circular polarization.

Figures 1(b) and 1(c) show the momentum distribution obtained from the solution of the TDSE for a short pulse. There, a shift of both the maximum and the bulk of the PMD toward higher momenta in the $p_y$ direction is observed. The difference between SFA and TDSE distributions is really a shift, not a rotation as would be the case in the conventional attoclock. To make this statement quantitative, we calculate the slope of a linear regression $p_x = a p_y + b$ through the relevant branch of the PMD. We find $a = 0.0183$ (corresponds to $1.05°$), while the relative shift of the distribution is $p_y^{\max}/p_x^{\max} = 0.155$. Hence, the shift is by far the dominant effect and the PMD is almost not rotated at all. In an experiment, this could allow for a simple calibration of the relative phase between the two fields, while the good agreement of the $p_x$ position of the maximum with the classical value (7) provides simple means for intensity calibration.

A common question related to the attoclock is whether the momentum shift is purely due to the effect that the atomic potential has on the outgoing electron after ionization, or whether a delay in ionization time has to be taken into account. More precisely, we want to answer the question whether the instantaneous ionization rate peaks at the same time as the electric field does. For this purpose we have to relate the ionization time to the observed photoelectron momentum, but also the observed signal at that momentum to the instantaneous ionization rate. The momentum distribution and ionization rate are generally not simply proportional to each other. In a classical picture involving trajectories starting at time $t$ with initial transverse momentum $v_\perp$, the momentum distribution can be written as

$$|\mathcal{M}(\mathbf{p})|^2 = \int dt \int dv_\perp W(t, v_\perp)\, \delta(\mathbf{p} - \mathbf{D}(t, v_\perp)), \tag{9}$$
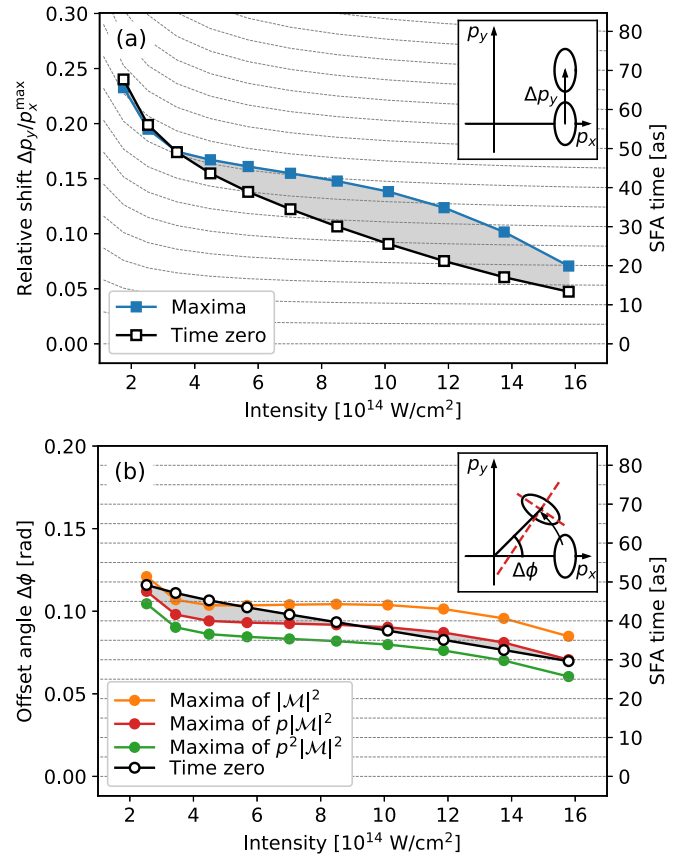


FIG. 2. (a) Relative shifts in the momentum distribution for the bicircular attoclock. The gray dashed lines give the relative shift that is, according to the SFA, Eq. (8), associated with a given time specified on the right vertical axis. (b) Offset angles for the circular attoclock including prefactors 1 (orange, upper curve), $p$ (red, middle curve), and $p^2$ (green, lower curve). Here, the (SFA) flow of time $d\phi/dt = \omega$ is the same for all intensities. In both panels, the open symbols indicate the momentum for ionization at maximum field (time zero).

where $W$ gives the instantaneous ionization probability per time per initial velocity and the deflection function $\mathbf{D}$ maps the initial conditions to the final momentum [53]. Resolving the $\delta$ function gives

$$|\mathcal{M}(\mathbf{p} = \mathbf{D}(t, v_\perp))|^2 = \frac{W(t, v_\perp)}{|\mathbf{D}'(t, v_\perp)|}. \tag{10}$$

Therefore, the maximum of the momentum distribution does not necessarily coincide with the maximum of the instantaneous ionization rate. The Jacobian has to be taken into account also. In the circular attoclock and neglecting the atomic potential, $|\mathbf{D}'(t, v_\perp)| = \omega p$. Previously it was found that including such geometrical factors can modify the measured angles significantly [50,51]. In the bicircular attoclock, however, the Jacobian of the deflection function is a constant to first order in the vicinity of the maximum and thus cannot influence the position of the maximum. This is because the second derivative of the vector potential vanishes at peak field strength when the ratio is chosen exactly 2:1 as is the case here (see Appendix B).

The shifts of the maxima are investigated systematically for various field strengths. The results are shown in Fig. 2(a)

(blue curve). Figure 2(b) shows the corresponding results for the circular attoclock (using a two-cycle $\cos^4$ envelope but otherwise the same parameters as in the bicircular case). There it is obvious that the angle at which the maximum is found depends on whether the geometrical factor is taken into account or not. This can be understood using a quadratic approximation of the PMD in the vicinity of its maximum which is characterized by two principal axes. A true rotation of the PMD would correspond to an external rotation of the peak position about the origin by a certain angle and an internal rotation of the principal axes by that same angle. In the circular attoclock we find that the two angles are not equal. The distribution is over-rotated. This is shown in the inset of Fig. 2(b). Multiplying the distribution with a radial factor then changes the angle at which the maximum is found. In the following we use the cylindrical factor according to the classical argument above but it should be noted that these strong variations raise questions toward the accuracy of the conventional attoclock. In contrast, for the bicircular attoclock this problem does not occur.

To relate the shifts to a possible delay in ionization time we employ a trajectory-free method we have developed recently [50]. There, the momentum distribution is expressed through the Dyson integral

$$\mathcal{M}(\mathbf{p}) = -i \int_0^T dt\, \mathcal{D}(\mathbf{p}, t), \qquad (11)$$

where

$$\mathcal{D}(\mathbf{p}, t) = \langle \psi_{\mathbf{p}}^{(-)} | U(T, t)[\mathbf{E}(t) \cdot \mathbf{x}] U_0(t, 0) | \psi_0 \rangle, \qquad (12)$$

$U_0$ denotes the field-free time-evolution operator, $U$ the full time-evolution operator, and $\psi_{\mathbf{p}}^{(-)}$ the incoming scattering state of momentum $\mathbf{p}$. In a fashion similar to the SFA, the ionization times and corresponding momenta are obtained as stationary points of the integrand via numerical solution of

$$\left.\frac{\partial}{\partial t} \ln \mathcal{D}(\mathbf{p}, t)\right|_{t=t_s} = \left.\frac{\partial_t \mathcal{D}(\mathbf{p}, t)}{\mathcal{D}(\mathbf{p}, t)}\right|_{t=t_s} = 0 \qquad (13)$$

in the complex plane. The difference to the SFA consists in taking the stationary points of the entire integrand (not just the action), as well as fully accounting for the atomic potential. The integrand is evaluated for all $\mathbf{p}$ at once using numerical wave-function propagation in complex time as described in [50]. For a given time $t$, the logarithmic derivative is then evaluated using three TDSE calculations and the second-order central-difference formula. Inserting a fixed momentum $\mathbf{p}$, we obtain a function of one complex variable $t$ for which roots can be found using Newton's method for a single variable. Here, convergence on an accuracy level comparable to the time step used in the TDSE calculations (approximately 0.1 attoseconds) can usually be achieved within three steps by reusing already obtained solutions for neighboring momenta. By varying the momentum in the $p_y$ direction we can find the relative shift that corresponds to the peak of the pulse, i.e., $\mathrm{Re}(t_s) = 0$, and also calculate a slice through the momentum distribution in saddle-point approximation. The latter is shown in Fig. 1(c). It agrees reasonably well with the exact TDSE result. The shifts are shown in Figs. 2(a) and 2(b). Alternatively, inserting the value of the momentum at the maximum
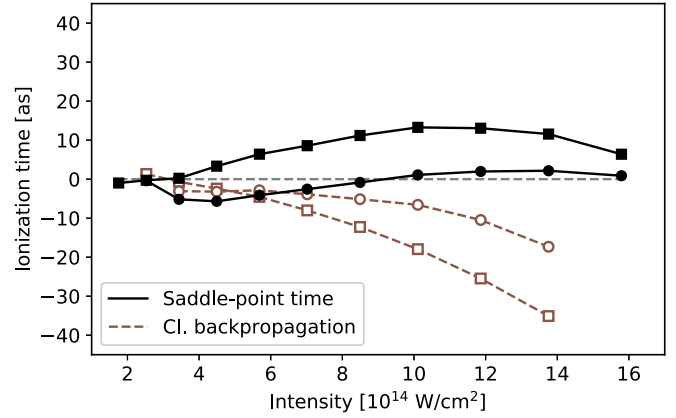


FIG. 3. Ionization times for the bicircular (squares) and circular (circles) attoclocks obtained by solving the saddle-point equation, Eq. (13) (black solid curves). The brown dashed curves give the most probable ionization time according to classical backpropagation.

of the PMD gives the most probable ionization time directly. This is shown in Fig. 3 and corresponds approximately to the difference between the shifts of the maxima and the shifts of time zero from Fig. 2 (gray area) on the SFA timescale. The bicircular attoclock shows an ionization time delay reaching more than 10 attoseconds that is not present in the circular case. Inspection of the saddle-point evaluation of the Dyson integral for the bicircular field shows that the prefactor $\propto 1/\sqrt{S''}$ with $S = i \ln \mathcal{D}$ causes such a shift, whereas no shift occurs when the prefactor is neglected. This prefactor can be interpreted as a measure of the time range contributing to the signal at a given momentum. The time range appears to be larger on the descending slope of the time-dependent field strength. Deeper investigation of this phenomenon deserves future work.

To make a further comparison, the bicircular attoclock also allows us to apply classical backpropagation [8–10] to quasi-linear polarization. In previous works, it has only been implemented for circular polarization. In truly linear polarization, classical backpropagation faces problems because electrons can come close to the parent ion where the correspondence between the quantum wave packet and the phase-space distribution of classical trajectories is lost. Additionally, interference in the electron wave packet makes the definition of a local velocity problematic. In the bicircular attoclock this is not the case. We backpropagate the interference-free ionized wave packet until the velocity of the Newtonian trajectory in the direction of the instantaneous electric field vanishes [54]. This gives a distribution of ionization times according to which classical trajectories would have to be launched to reproduce the quantum-mechanical momentum distribution. The maxima of these distributions for the circular and bicircular case are shown in Fig. 3. Unlike the saddle-point prescription of ionization time (13), the classical prescription actually produces dominant ionization times before the time of peak field strength. This was also the case in [6,8,55]. For small intensities, all curves consistently point to zero ionization time delay within a few attoseconds. We believe that the result of very small or negative times is a common feature of methods involving Newtonian trajectories that tunnel out from the atom

with zero initial parallel velocity. There is another class of methods yielding instead large positive times: the Wigner time in Camus *et al.* [6], the ionization time of Bohmian trajectories [56,57] and the time delay of Teeny *et al.* [58], which can be understood as indicating the time when the flow of probability density at the tunnel exit is maximized. As argued by Ni *et al.* [9], large positive times are a common feature of methods where the time definition is related to the tunnel exit position rather than zero starting velocity. For most of the cases we have studied, our fully quantum-mechanical saddle-point times are closer to zero than the results from any of the above-mentioned methods (excluding here the analytical *R*-matrix theory by Torlina *et al.* [5], where the $p^2$ prescription was used to determine the maximum of the momentum distribution). This may be interpreted such that a treatment as accurate as possible yields the smallest deviations from the peak of the field, which appears physically reasonable to the authors. A completely different approach that uses functional derivatives of the ionization yield with respect to the field shape also supports vanishing ionization time delay by a symmetry argument [59].

To conclude, we have demonstrated that the ionization step in quasilinear polarization can be probed in a rescattering-free and interference-free setup using attoclock techniques and we have provided the main equations required to calibrate the clock. Our scheme provides highly accurate information on the ionization dynamics around the peak of the laser field unlike approaches involving truly linearly polarized fields. Investigating the shifts in the PMD with regard to the time of ionization, we found a small delay with respect to the time of peak field strength that is not present in circular polarization. The presented results were obtained for 1131 nm wavelength of the fundamental field, but similar results, including a small positive delay, are found at 800 nm, which is widely used in two-color experiments.

In the future, the bicircular attoclock could be used to study orientation-dependent ionization times in molecules as the electric field has a well-defined direction in the vicinity of peak field strength. Additionally, existing parallel or orthogonal two-color schemes could be combined with the bicircular attoclock to achieve interference-free and rescattering-free measurements of momentum-resolved ionization times in quasilinear polarization.

## APPENDIX A: SPEED OF THE CLOCK

Evaluating (6) at time zero and minimal imaginary part $t_i$ of the ionization time, i.e., vanishing square root,

gives

$$\frac{dp_y}{dt} = \frac{2E_0}{\sqrt{5}}\left(\cosh(\omega t_i) + \frac{1}{2}\cosh(2\omega t_i)\right) \tag{A1}$$

and

$$\sqrt{2I_p} = \frac{2E_0}{\sqrt{5}\,\omega}\left(\sinh(\omega t_i) + \frac{1}{4}\sinh(2\omega t_i)\right). \tag{A2}$$

Then we can approximate

$$\cosh(\omega t_i) + \tfrac{1}{2}\cosh(2\omega t_i) \approx \tfrac{3}{2}\cosh(\omega_{\text{eff}} t_i) \tag{A3}$$

and

$$\sinh(\omega t_i) + \frac{1}{4}\sinh(2\omega t_i) \approx \frac{3}{2\sqrt{2}}\sinh(\omega_{\text{eff}} t_i) \tag{A4}$$

to get

$$\frac{dp_y}{dt} \approx E_{\text{peak}}\cosh(\omega_{\text{eff}} t_i) \tag{A5}$$

and

$$\sqrt{2I_p} \approx \frac{E_{\text{peak}}}{\omega_{\text{eff}}}\sinh(\omega_{\text{eff}} t_i). \tag{A6}$$

Combining the two equations gives

$$\frac{dp_y}{dt} \approx E_{\text{peak}}\sqrt{1 + \gamma_{\text{eff}}^2}. \tag{A7}$$

Finally, the absolute value of the momentum is

$$p_x^{\text{max}} \approx \frac{E_{\text{peak}}}{2\omega}. \tag{A8}$$

## APPENDIX B: JACOBIAN FACTORS

Disregarding the atomic potential, the classical deflection function can be written explicitly as

$$\mathbf{p}(t, v_\perp) = -\mathbf{A}(t) + v_\perp \hat{\mathbf{E}}_\perp(t), \tag{B1}$$

where

$$\hat{\mathbf{E}}_\perp = \frac{1}{\sqrt{E_x^2 + E_y^2}}\begin{pmatrix} E_y \\ -E_x \end{pmatrix}. \tag{B2}$$

The second derivatives at $v_\perp = 0$ are

$$\begin{aligned} \frac{\partial^2 \mathbf{p}}{\partial t^2} &= -\mathbf{A}'', \quad \frac{\partial^2 \mathbf{p}}{\partial v_\perp^2} = 0, \\ \frac{\partial^2 \mathbf{p}}{\partial t\, \partial v_\perp} &= \frac{(\mathbf{E}_\perp \cdot \mathbf{A}'')}{|\mathbf{E}|^3}\mathbf{E}. \end{aligned} \tag{B3}$$

In the bicircular attoclock $\mathbf{A}''(0) = 0$, so all second derivatives vanish and the Jacobian, which consists of first derivatives, is constant to first order in $t$ and $v_\perp$ in the vicinity of $t, v_\perp = 0$.

[1] P. Eckle, M. Smolarski, P. Schlup, J. Biegert, A. Staudte, M. Schöffler, H. G. Muller, R. Dörner, and U. Keller, Attosecond angular streaking, Nat. Phys. **4**, 565 (2008).

[2] P. Eckle, A. N. Pfeiffer, C. Cirelli, A. Staudte, R. Dörner, H. G. Muller, M. Büttiker, and U. Keller, Attosecond ionization and tunneling delay time measurements in helium, Science **322**, 1525 (2008).

[3] A. N. Pfeiffer, C. Cirelli, M. Smolarski, D. Dimitrovski, M. Abu-samha, L. B. Madsen, and U. Keller, Attoclock reveals natural coordinates of the laser-induced tunnelling current flow in atoms, Nat. Phys. **8**, 76 (2012).

[4] A. S. Landsman, M. Weger, J. Maurer, R. Boge, A. Ludwig, S. Heuser, C. Cirelli, L. Gallmann, and U. Keller, Ultrafast resolution of tunneling delay time, Optica **1**, 343 (2014).

[5] L. Torlina, F. Morales, J. Kaushal, I. Ivanov, A. Kheifets, A. Zielinski, A. Scrinzi, H. G. Muller, S. Sukiasyan, M. Ivanov, and O. Smirnova, Interpreting attoclock measurements of tunnelling times, Nat. Phys. **11**, 503 (2015).

[6] N. Camus, E. Yakaboylu, L. Fechner, M. Klaiber, M. Laux, Y. Mi, K. Z. Hatsagortsyan, T. Pfeifer, C. H. Keitel, and R. Moshammer, Experimental Evidence for Quantum Tunneling Time, Phys. Rev. Lett. **119**, 023201 (2017).

[7] V. P. Majety and A. Scrinzi, Absence of electron correlation effects in the Helium attoclock setting, J. Mod. Opt. **64**, 1026 (2017).

[8] H. Ni, U. Saalmann, and J. M. Rost, Tunneling Ionization Time Resolved by Backpropagation, Phys. Rev. Lett. **117**, 023002 (2016).

[9] H. Ni, U. Saalmann, and J. M. Rost, Tunneling exit characteristics from classical backpropagation of an ionized electron wave packet, Phys. Rev. A **97**, 013426 (2018).

[10] H. Ni, N. Eicke, C. Ruiz, J. Cai, F. Oppermann, N. I. Shvetsov-Shilovski, and L. W. Pi, Tunneling criteria and a nonadiabatic term for strong-field ionization, Phys. Rev. A **98**, 013411 (2018).

[11] J. L. Krause, K. J. Schafer, and K. C. Kulander, High-Order Harmonic Generation from Atoms and Ions in the High Intensity Regime, Phys. Rev. Lett. **68**, 3535 (1992).

[12] P. B. Corkum, Plasma Perspective on Strong Field Multiphoton Ionization, Phys. Rev. Lett. **71**, 1994 (1993).

[13] T. Zuo, A. D. Bandrauk, and P. B. Corkum, Laser-induced electron diffraction: A new tool for probing ultrafast molecular dynamics, Chem. Phys. Lett. **259**, 313 (1996).

[14] M. Lein, J. P. Marangos, and P. L. Knight, Electron diffraction in above-threshold ionization of molecules, Phys. Rev. A **66**, 051404 (2002).

[15] M. Meckel, D. Comtois, D. Zeidler, A. Staudte, D. Pavičić, H. C. Bandulet, H. Pépin, J. C. Kieffer, R. Dörner, D. M. Villeneuve, and P. B. Corkum, Laser-induced electron tunneling and diffraction, Science **320**, 1478 (2008).

[16] D. Ray, B. Ulrich, I. Bocharova, C. Maharjan, P. Ranitovic, B. Gramkow, M. Magrakvelidze, S. De, I. V. Litvinyuk, A. T. Le, T. Morishita, C. D. Lin, G. G. Paulus, and C. L. Cocke, Large-Angle Electron Diffraction Structure in Laser-Induced Rescattering from Rare Gases, Phys. Rev. Lett. **100**, 143002 (2008).

[17] M. Okunishi, T. Morishita, G. Prümper, K. Shimada, C. D. Lin, S. Watanabe, and K. Ueda, Experimental Retrieval of Target Structure Information from Laser-Induced Rescattered Photoelectron Momentum Distributions, Phys. Rev. Lett. **100**, 143001 (2008).

[18] T. M. Yan, S. V. Popruzhenko, M. J. J. Vrakking, and D. Bauer, Low-Energy Structures in Strong Field Ionization Revealed by Quantum Orbits, Phys. Rev. Lett. **105**, 253002 (2010).

[19] M. Li, J. W. Geng, H. Liu, Y. Deng, C. Wu, L. Y. Peng, Q. Gong, and Y. Liu, Classical-Quantum Correspondence for Above-Threshold Ionization, Phys. Rev. Lett. **112**, 113002 (2014).

[20] N. I. Shvetsov-Shilovski, M. Lein, L. B. Madsen, E. Räsänen, C. Lemell, J. Burgdörfer, D. G. Arbó, and K. Tőkési, Semiclassical two-step model for strong-field ionization, Phys. Rev. A **94**, 013415 (2016).

[21] A. M. Perelomov, V. S. Popov, and M. V. Terent'ev, Ionization of atoms in an alternating electric field, Sov. Phys. JETP **23**, 924 (1966).

[22] C. Z. Bisgaard and L. B. Madsen, Tunneling ionization of atoms, Am. J. Phys. **72**, 249 (2004).

[23] P. Salières, B. Carré, L. L. Déroff, F. Grasbon, G. G. Paulus, H. Walther, R. Kopold, W. Becker, D. B. Milošević, A. Sanpera, and M. Lewenstein, Feynman's path-integral approach for intense-laser-atom interactions, Science **292**, 902 (2001).

[24] D. B. Milošević, G. G. Paulus, D. Bauer, and W. Becker, Above-threshold ionization by few-cycle pulses, J. Phys. B: At., Mol. Opt. Phys. **39**, R203 (2006).

[25] I. Barth and O. Smirnova, Nonadiabatic tunneling in circularly polarized laser fields: Physical picture and calculations, Phys. Rev. A **84**, 063415 (2011).

[26] S. V. Popruzhenko, Keldysh theory of strong field ionization: History, applications, difficulties and perspectives, J. Phys. B: At., Mol. Opt. Phys. **47**, 204001 (2014).

[27] S. Eckart, M. Kunitski, M. Richter, A. Hartung, J. Rist, F. Trinter, K. Fehre, N. Schlott, K. Henrichs, L. P. H. Schmidt, T. Jahnke, M. Schöffler, K. Liu, I. Barth, J. Kaushal, F. Morales, M. Ivanov, O. Smirnova, and R. Dörner, Ultrafast preparation and detection of ring currents in single atoms, Nat. Phys. **14**, 701 (2018).

[28] A. Rudenko, K. Zrost, T. Ergler, A. B. Voitkiv, B. Najjari, V. L. B. de Jesus, B. Feuerstein, C. D. Schröter, R Moshammer, and J. Ullrich, Coulomb singularity in the transverse momentum distribution for strong-field single ionization, J. Phys. B: At., Mol. Opt. Phys. **38**, L191 (2005).

[29] D. Comtois, D. Zeidler, H. Pépin, J. C. Kieffer, D. M. Villeneuve, and P. B. Corkum, Observation of Coulomb focusing in tunnelling ionization of noble gases, J. Phys. B: At., Mol. Opt. Phys. **38**, 1923 (2005).

[30] D. G. Arbó, S. Yoshida, E. Persson, K. I. Dimitriou, and J. Burgdörfer, Interference Oscillations in the Angular Distribution of Laser-Ionized Electrons near Ionization Threshold, Phys. Rev. Lett. **96**, 143003 (2006).

[31] D. G. Arbó, K. I. Dimitriou, E. Persson, and J. Burgdörfer, Sub-Poissonian angular momentum distribution near threshold in atomic ionization by short laser pulses, Phys. Rev. A **78**, 013406 (2008).

[32] D. G. Arbó, E. Persson, and J. Burgdörfer, Time double-slit interferences in strong-field tunneling ionization, Phys. Rev. A **74**, 063407 (2006).

[33] F. Lindner, M. G. Schätzel, H. Walther, A. Baltuška, E. Goulielmakis, F. Krausz, D. B. Milošević, D. Bauer, W. Becker, and G. G. Paulus, Attosecond Double-Slit Experiment, Phys. Rev. Lett. **95**, 040401 (2005).

[34] N. Dudovich, O. Smirnova, J. Levesque, Y. Mairesse, M. Y. Ivanov, D. M. Villeneuve, and P. B. Corkum, Measuring and controlling the birth of attosecond XUV pulses, Nat. Phys. **2**, 781 (2006).

[35] S. Skruszewicz, J. Tiggesbäumker, K. H. Meiwes-Broer, M. Arbeiter, T. Fennel, and D. Bauer, Two-Color Strong-Field

Photoelectron Spectroscopy and the Phase of the Phase, Phys. Rev. Lett. **115**, 043001 (2015).

[36] G. Porat, G. Alon, S. Rozen, O. Pedatzur, M. Krüger, D. Azoury, A. Natan, G. Orenstein, B. D. Bruner, M. J. J. Vrakking, and N. Dudovich, Attosecond time-resolved photo-electron holography, Nat. Commun. **9**, 2805 (2018).

[37] J. Henkel and M. Lein, Analysis of electron trajectories with two-color strong-field ionization, Phys. Rev. A **92**, 013422 (2015).

[38] N. Eicke and M. Lein, Extracting trajectory information from two-color strong-field ionization, J. Mod. Opt. **64**, 981 (2017).

[39] D. Shafir, H. Soifer, B. D. Bruner, M. Dagan, Y. Mairesse, S. Patchkovskii, M. Y. Ivanov, O. Smirnova, and N. Dudovich, Resolving the time when an electron exits a tunnelling barrier, Nature **485**, 343 (2012).

[40] J. Zhao and M. Lein, Determination of Ionization and Tunneling Times in High-Order Harmonic Generation, Phys. Rev. Lett. **111**, 043901 (2013).

[41] G. G. Paulus, W. Nicklich, H. Xu, P. Lambropoulos, and H. Walther, Plateau in Above Threshold Ionization Spectra, Phys. Rev. Lett. **72**, 2851 (1994).

[42] H. Eichmann, A. Egbert, S. Nolte, C. Momma, B. Wellegehausen, W. Becker, S. Long, and J. K. McIver, Polarization-dependent high-order two-color mixing, Phys. Rev. A **51**, R3414 (1995).

[43] D. B. Milošević and W. Becker, Improved strong-field approximation and quantum-orbit theory: Application to ionization by a bicircular laser field, Phys. Rev. A **93**, 063418 (2016).

[44] E. Hasović, W. Becker, and D. B. Milošević, Electron rescattering in a bicircular laser field, Opt. Express **24**, 6413 (2016).

[45] V. H. Hoang, V. H. Le, C. D. Lin, and A. T. Le, Retrieval of target structure information from laser-induced photoelectrons by few-cycle bicircular laser fields, Phys. Rev. A **95**, 031402 (2017).

[46] S. Eckart, M. Richter, M. Kunitski, A. Hartung, J. Rist, K. Henrichs, N. Schlott, H. Kang, T. Bauer, H. Sann, L. P. H. Schmidt, M. Schöffler, T. Jahnke, and R. Dörner, Nonsequential Double Ionization by Counterrotating Circularly Polarized Two-Color Laser Fields, Phys. Rev. Lett. **117**, 133202 (2016).

[47] C. A. Mancuso, K. M. Dorney, D. D. Hickstein, J. L. Chaloupka, X. M. Tong, J. L. Ellis, H. C. Kapteyn, and M. M. Murnane, Observation of ionization enhancement in two-color circularly polarized laser fields, Phys. Rev. A **96**, 023402 (2017).

[48] S. Eckart, M. Kunitski, I. Ivanov, M. Richter, K. Fehre, A. Hartung, J. Rist, K. Henrichs, D. Trabert, N. Schlott, L. P. H. Schmidt, T. Jahnke, M. S. Schöffler, A. Kheifets, and R. Dörner, Subcycle interference upon tunnel ionization by counter-rotating two-color fields, Phys. Rev. A **97**, 041402 (2018).

[49] M. Han, P. Ge, Y. Shao, Q. Gong, and Y. Liu, Attoclock Photoelectron Interferometry with Two-Color Corotating Circular Fields to Probe the Phase and the Amplitude of Emitting Wave Packets, Phys. Rev. Lett. **120**, 073202 (2018).

[50] N. Eicke and M. Lein, Trajectory-free ionization times in strong-field ionization, Phys. Rev. A **97**, 031402 (2018).

[51] J. Kaushal, F. Morales, L. Torlina, M. Ivanov, and O. Smirnova, Spin–orbit Larmor clock for ionization times in one-photon and strong-field regimes, J. Phys. B: At., Mol. Opt. Phys. **48**, 234002 (2015).

[52] M. Lein, E. K. U. Gross, and V. Engel, Intense-Field Double Ionization of Helium: Identifying the Mechanism, Phys. Rev. Lett. **85**, 4707 (2000).

[53] A. Kästner, U. Saalmann, and J. M. Rost, Electron-Energy Bunching in Laser-Driven Soft Recollisions, Phys. Rev. Lett. **108**, 033201 (2012).

[54] Since the SFA predicts nonvanishing parallel exit velocities for linear polarization it is not clear whether the current tunnel-exit criterion that relies on vanishing velocities is ideal. Some progress toward a more general criterion has already been made in [10].

[55] M. Lein, Streaking analysis of strong-field ionisation, J. Mod. Opt. **58**, 1188 (2011).

[56] T. Zimmermann, S. Mishra, B. R. Doran, D. F. Gordon, and A. S. Landsman, Tunneling Time and Weak Measurement in Strong Field Ionization, Phys. Rev. Lett. **116**, 233603 (2016).

[57] N. Douguet and K. Bartschat, Dynamics of tunneling ionization using Bohmian mechanics, Phys. Rev. A **97**, 013402 (2018).

[58] N. Teeny, E. Yakaboylu, H. Bauke, and C. H. Keitel, Ionization Time and Exit Momentum in Strong-Field Tunnel Ionization, Phys. Rev. Lett. **116**, 063003 (2016).

[59] I. A. Ivanov, C. Hofmann, L. Ortmann, A. S. Landsman, C. H. Nam, and K. T. Kim, Instantaneous ionization rate as a functional derivative, Commun. Phys. **1**, 81 (2018).